Depolarization Sensing by Orthogonality Breaking: a microwave-photonics approach for snapshot polarimetric imaging

Julien Fade, Emmanuel Schaub, Mehdi Alouini

OPTRO-2014-2967942

DEPOLARIZATION SENSING BY ORTHOGONALITY BREAKING: A MICROWAVE-PHOTONICS APPROACH FOR SNAPSHOT POLARIMETRIC IMAGING

Julien Fade[(1)], Emmanuel Schaub[(2)], Mehdi Alouini[(3)]

[(1)] Institut de Physique de Rennes, Université de Rennes 1-CNRS, Campus de Beaulieu, 35 042 Rennes, France, julien.fade@univ-rennes1.fr
[(2)] Institut de Physique de Rennes, Université de Rennes 1-CNRS, Campus de Beaulieu, 35 042 Rennes, France, emmanuel.schaub@univ-rennes1.fr
[(3)] Institut de Physique de Rennes, Université de Rennes 1-CNRS, Campus de Beaulieu, 35 042 Rennes, France, mehdi.alouini@univ-rennes1.fr

KEYWORDS: active imaging, polarimetric imaging, laser, microwave photonics, remote sensing.

ABSTRACT:

We report a new depolarization sensing modality (DSOB), based on the concept of polarization orthogonality breaking, enabling direct measurement of a polarimetric contrast from a single measurement. The principle of this technique is described, as well as its benefits (compatibility with remote sensing through fibers, spectral agility…). Experimental validation of this technique on a fibred setup is extensively described and confirms its appropriateness for remote sensing through optical fibers. We eventually present the first DSOB images obtained in the visible range on a confocal microscope setup. The acquisition times reported are encouraging for future implementation in real-time.

1. INTRODUCTION

Active imaging is a field of research with important outcomes for defense applications, ranging from homeland security applications, surveillance, and protection of strategic targets to anti-piracy or soldier vision enhancement in complex hostile environment. In this context, a fundamental question is the search for the most relevant imaging modalities involving nonstandard physical properties of light – i.e., other than a standard reflectance intensity image. Polarization sensitive imaging techniques have long been identified as potential solutions to improve the performance of surveillance systems for concealed targets detection [1-9] or objects recognition [10, 11]. In the field of active imaging for defense applications, a number of polarimetric systems include multispectral capabilities in order to simultaneously record spectral signatures and polarimetric response of the scene [3, 5, 12, 13]. If both information channels (polarimetric and spectral) can be exploited independently to improve the specificity of target signatures, it has also been demonstrated that merging those two information channels can reveal relevant and characteristic features of materials (discrimination between metallic/man-made targets and vegetation background clutter) [2-4, 8, 11].

However, the diffusion of polarimetric imagers in operational systems (defense or medical) or in everyday applications has been so far restrained by a number of technological bottle-necks, which are:

(a) The difficulty to perform real-time and/or wavelength agile measurements: multiple intensity measurements are needed, often with moving polarizers/waveplates thus requiring image registration;

(b) The lack of range: since the requested signature is a polarimetric contrast, the final image quality relies on one's ability to detect low intensity differences, that is, on the possibility to shine the scene with sufficiently high optical powers.

(c) The inadequacy of existing techniques to remote-sensing through optical waveguides, due to the lack of polarization control in fibers.

In this context, we recently proposed to revisit the way of performing depolarization measurements using a novel concept of field orthogonality breaking (Depolarization Sensing by Orthogonality Breaking (DSOB)), which provides a direct characterization of the depolarization strength of a material from a single measurement [14]. This technique, inspired by a microwave photonics approach, uses a superposition of two orthogonally polarized modes with a slight frequency detuning to enlighten the sample. Using such illumination, it can be shown that the depolarizing strength of a sample is directly retrieved from a single measurement of the beat note intensity, appearing at the difference frequency. In other words, the depolarization strength of a given material can be recovered from the way this material breaks the orthogonality between two incident orthogonal states. In addition, it must be noted that this technique is well suited for endoscopic remote sensing, being inherently insensitive to fiber/endoscope birefringences which preserve polarimetric orthogonality.

This paper is organized as follows: in Section 2, some basics on polarimetry and polarization contrast imaging are recalled. Then the DSOB principle is described in Section 3. Its validation with a first experimental implementation is detailed in Section 4. We report in Section 5 the realization of the first DSOB polarimetric contrast images before providing conclusions in section 6.

2. BACKGROUND ON POLARIMETRIC IMAGING

Polarimetric imaging consists in analyzing and mapping the state of polarization of light emitted or backscattered by one or several objects in a scene. Many application domains have been identified since the development of the first polarimetric imagers. A non-exhaustive list would mention microscopy [15-17] (linear or nonlinear), surfaces/interfaces and materials characterization [18, 19], strain detection [20], computer vision [21] or enhanced vision through turbid media [22, 23], target detection [1-4, 24, 25] and biomedical diagnosis [26-33].

Polarimetric imagers often include a light source, whose state of polarization is well controlled, and which is used to shine the scene under investigation (active imaging). The detection part of the system must be polarization-sensitive and able to provide two-dimensional information on the polarization of light scattered at each point of the scene. Many acquisition procedures and techniques of varying complexity have been identified for various purposes, with different advantages and drawbacks. The most exhaustive is Mueller imaging which analyses the polarization state of backscattered or transmitted light as a function of the illuminating light polarization. This technique, requiring the acquisition of 16 images (16 terms of the 4x4 real Mueller matrix), is useful when the sample to be characterized has –in addition to pure depolarization– a measurable effect on light polarization due to birefringence, optical activity, diattenuation,… This imaging modality has been used for biological tissues characterization [26, 28, 32].

From a practical point of view however, the full characterization of this matrix, or of the polarization state of backscattered light (which requires measuring the 4-dimensional Stokes vector in each point of the scene) sometimes provides the end-user with a superfluous amount of information. A part of this information is thus often discarded through data processing to supply a highly contrasted low-dimensional (or even scalar) final image to the end-user or to the higher-level processing task (segmentation, detection, recognition…). Such trend towards data reduction justifies the large variety of simplified polarimetric imaging systems that have been proposed, which all aim at reducing costs and duration of polarimetric image acquisitions [5, 12, 21, 24, 29, 34, 35].

Therefore, in numerous applications, a more pragmatic approach consists in measuring a limited number of images and displaying a single polarimetric contrast image to the end-user. Mostly often, the contrast parameter - or *figure of merit* - considered is the degree of polarization (DOP), which will be denoted $\mathcal{P}$ in the following. This scalar quantity makes it possible to distinguish totally polarized light ($\mathcal{P}$ =1) from partially polarized light

(0<$\mathcal{P}$<1). Measuring $\mathcal{P}$ usually necessitates the full characterization of the Stokes vector, which is bijectively related to the components of the polarization matrix Γ describing second-order correlations and fluctuations of the field vectorial components [36].

Practically speaking, a wide majority of materials can be considered as purely depolarizing [2, 24] when considered at a macroscopic scale. In this case, the measurement procedure can be limited to the acquisition of two images through different configurations of a linear analyzer, first aligned with the illumination source polarization (acquisition of image $I_{//}$), and then rotated in the orthogonal direction (acquisition of image $I_{\perp}$). Under the assumption of purely depolarizing sample, the DOP map can be deduced by computing the following contrast image

$$OSC = \frac{I_{//} - I_{\perp}}{I_{//} + I_{\perp}}. \qquad (1)$$

This simplified imaging modality is usually termed "Orthogonal States Contrast (OSC) Imaging" (OSCI) in the active imaging community [37].

It is eventually important to note that, as in biomedical applications, or for pattern recognition, display of the polarimetric data to the end-user is often reduced to a single contrast image in a number of active imaging applications. As a consequence, simplified imaging systems focusing on scalar polarimetric figures of merit (DOP or OSC) have been widely used in teledetection and military applications. In this context, original methods taking advantage of speckle statistics to supply DOP images from two [35] and even one image acquisition(s) [34, 38] have been addressed. However, it was shown that such simplification is at the expense of a degradation of the spatial resolution of the image [38].

More generally, these last examples demonstrate that acquiring a large number of polarimetric images is not necessarily optimal for contrast maximization. Indeed, in addition to complexity and measurement time increase, computing the best data combination of the 16 Mueller matrix measurements for contrast enhancement is not necessarily straightforward. In some cases indeed, direct determination of the contrast parameter of interest for a specified task could be more appropriate.

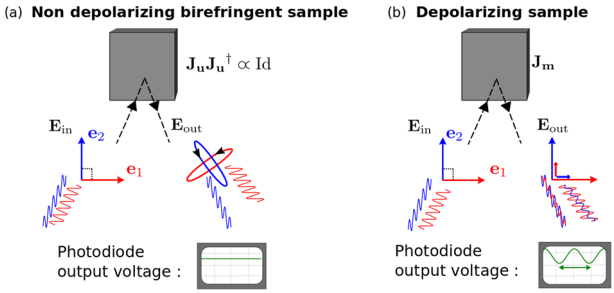

Figure 1. Principle of the DSOB technique.

3. PRINCIPLE OF DSOB

The concept of Depolarization Sensing by Orthogonality Breaking is based on the preparation of a specific probe light beam, which is used to enlighten the target (or sample) to characterize. This probe beam contains two light waves with respective optical frequencies ν_1 and ν_2 which are slightly detuned by a quantity $\Delta\nu=\nu_1-\nu_2$. These two waves can be any deterministic states of polarization $\mathbf{e}_1$ and $\mathbf{e}_2$ (fully polarized fields), but these two states have to be orthogonal to each other in a mathematical sense. This light field can thus be written

$$\mathbf{E}_{in}=\frac{E_0}{\sqrt{2}} e^{-2i\pi\nu_1}[\mathbf{e}_1+e^{-2i\pi\Delta\nu}\mathbf{e}_2]. \qquad (2)$$

The intensity of this field is constant in time since the two frequencies contained in the light field do not beat with each other, since lying in two orthogonal polarization states. When such beam $\mathbf{E}_{in}$ is made to interact with a sample, the action of the latter on the field polarization state can be modeled by a Jones matrix $\mathbf{J}_s$, and thus $\mathbf{E}_{out}=\mathbf{J}_s\,\mathbf{E}_{in}$. Two situations can then be encountered:

- when $\mathbf{J}_s$ is a deterministic unitary Jones matrix $\mathbf{J}_s=\mathbf{J}_u$ (or proportional to a unitary Jones matrix, up to a isotropic absorption factor denoted ρ), the intensity of the output field is given by $I_{out}=\rho\,|E_0|^2$, which is still constant in time, since orthogonality (in the mathematical sense) between the two output field states $\mathbf{J}_u\mathbf{e}_1$ and $\mathbf{J}_u\mathbf{e}_2$ is maintained with unitary transformations. This situation occurs with birefringent samples or samples showing optical activity. This property, illustrated in Fig. 1.(a) is

valid provided no significant dispersion appears between frequencies ν_1 and ν_2. This is very unlikely to occur in practice since $\Delta\nu$ will not exceed tens of gigahertz for the beat note to be detectable on a photodetector [14].

- Now, when the sample is depolarizing, or in the presence of absorption anisotropy, the mathematical orthogonality is broken when light interacts with the sample. For instance, the Jones matrix describing absorption anisotropy along the X/Y direction and with anisotropy factor τ is given by

$$\mathbf{J}_{an}=\sqrt{\rho}\begin{pmatrix}\sqrt{1+\tau} & 0\\ 0 & \sqrt{1-\tau}\end{pmatrix}. \qquad (3)$$

In this case, it can be easily shown that with eigen polarizations oriented at angle θ with respect to the X direction, and with ellipticity δ, the output intensity is given by $I_{out} = \rho I_0 [1 + (\tau \sin 2\theta \cos\delta) \cos(2\pi\Delta\nu t)]$. From the latter equation, it can be observed that absorption anisotropy gives rise in general to a beat note term in the intensity, due to orthogonality breaking between the two eigen polarizations (see Fig. 1.(b)). Thus the dichroic nature of the target can be easily and directly detected on the output beam intensity itself, provided the photodetector used has sufficient bandpass to measure the intensity component at the beat note frequency $\Delta\nu=\nu_1-\nu_2$.

Let us now consider the case of a purely depolarizing sample, which is conventionally described by a diagonal Mueller matrix **M**=diag [1, $\mathcal{P}$, $\mathcal{P}$, $\mathcal{P}$]. When enlightened by a totally polarized beam $\mathbf{e}_{in}$, such depolarizing sample partially transfers some of the input field intensity onto all the other polarization directions. This can also be phenomenologically described by a partial projection on the orthogonal polarization direction $\mathbf{e}_{in}^{\perp}$, which projection we proposed to model with the following Jones matrix [14]

$$\mathbf{J}_{dep}=\sqrt{\rho}R_{in}^{\dagger}\begin{pmatrix}1 & \alpha\\ \alpha & 1\end{pmatrix}R_{in}. \qquad (4)$$

In the above equation, the unitary matrix R_{in} corresponds to a generalized polarization rotation matrix, mapping the transverse field eigenbasis $\{\mathbf{e}_1, \mathbf{e}_2\} = \{\mathbf{e}_{in}, \mathbf{e}_{in}\}$ into the standard linear transverse field basis $\{\mathbf{e}_X, \mathbf{e}_Y\}$. When the probe beam interacts with such purely depolarizing sample, the output intensity is then $I_{out}= \rho I_0[(1+\alpha^2) + (2\alpha)\cos(2\pi\Delta\nu t)]$, thus showing that the depolarizing nature of a sample is assessed from a direct measurement of the beat note intensity. In practice, it is interesting to normalize the detected intensity at frequency $\Delta\nu$ by the DC component of the intensity. It can indeed be shown [14] that the power contrast $C^{\Delta\nu}{}_{out}= P^{\Delta\nu}{}_{out} / P^{DC}{}_{out}$ can be directly linked to the DOP of the sample by

$$C_{out}^{\Delta\nu}=\frac{P_{out}^{\Delta\nu}}{P_{out}^{DC}}=1-\mathcal{P}^2. \qquad (5)$$

Moreover, in the case of purely depolarizing sample, this result is still valid after the beam has undergone deterministic unitary transformations on its propagation between the source and the target.

It is indeed clear from the above calculations that the DSOB principle is in essence insensitive to birefringence and polarization rotation, thus enabling remote sensing through optical fibers, in which stress- or torsion-induced birefringences are usually highly detrimental to usual polarimetric measurements [14].

4. Experimental validation

4.1. Implementation at 1.5 µm with a dual-frequency laser

To experimentally illustrate and validate the DSOB principle, we implemented a diode-pumped (Er,Yb)-doped glass 4-cm-long external cavity laser emitting at 1550 nm used to prepare the field in the appropriate probe state described above. An intracavity 40-µm-thick silica etalon was used to ensure single-longitudinal mode oscillation. Moreover, a 500-µm-thick YVO_4 crystal, cut at 45° of its optical axis, was inserted into the laser cavity in order to favor dual-frequency operation of the laser [39, 40]. In this configuration sketched in Fig. 2, the output field is generated along two polarization eigenstates $\mathbf{e}_1$ and $\mathbf{e}_2$ defined by the eigen axes of the YVO_4 crystal, each of it oscillating at a given frequency ν_1 and ν_2, the frequency difference $\Delta\nu$ being proportional to the cavity free-spectral-range and to the intracavity phase anisotropy between the two eigenstates [39]. By slightly tilting the etalon and the YVO_4 crystal, it was possible to set this frequency

difference to a value compatible with the detection setup, namely within the radio-frequency (RF) range, i.e., $\Delta\nu < 2$ GHz. In this configuration, the laser provided an output power of 1.8 mW equally distributed on two orthogonal states of polarization $\mathbf{e}_1$ and $\mathbf{e}_2$ (horizontal and vertical), with a pump power of approximately 130 mW [14].

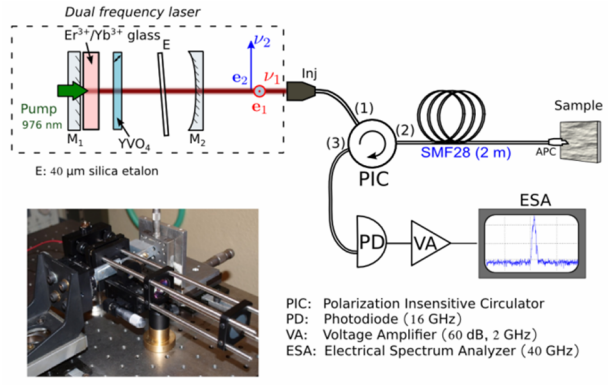

Figure 2. Schematic of the validation fibred setup at 1.55 µm. Inset: photography of the dual-frequency orthogonal polarizations laser used.

The DSOB principle was first tested in a fibred configuration which is represented in Fig. 2. For that purpose, the dual-frequency probe beam was injected and guided into a 2 m-long single-mode optical fiber (SMF28) before illuminating a target. The backscattered light was back propagated into the same fiber, and analyzed through a polarization-insensitive circulator (PIC) and directed on a high-band pass (16 GHz) photodiode (PD). A high-gain (60 dB, 2 GHz cutoff frequency) voltage amplifier and a 40 GHz band pass electrical spectrum analyzer (ESA) were finally used to analyze the detected signal. At this level, it must be noticed that this measurement setup does not require any component to be inserted at the distal fiber end and may thus be directly adapted to commercial endoscopes. More importantly, no polarizing or birefringent elements are needed in the illumination / detection setup. As a consequence, the spectral range of the setup is therefore only limited by the source, the photodiode, and the fiber spectral excursions. The DSOB technique could therefore easily provide spectrally resolved polarimetric measurements. This ability can be interesting for target detection which has proved efficient when spectro-polarimetric measurements were accessible, or for materials characterization and biomedical diagnosis.

Table 1. Calibration of the polarimetric contrast in various experimental conditions

	Polarimetric DSOB contrast
After injection in SMF28	34 dB
After 25 km propagation	25 dB
Through fibred circulator	28 dB
Distal fibred mirror + circulator	27 dB

4.2. Calibration

To estimate the available dynamics of such polarimetric measurement, we first analyzed the maximum "polarimetric orthogonality contrast" available with our setup. This measurement was done by comparing the residual beat note power $P^{\Delta\nu}_{res}$ (caused by imperfect orthogonality between the polarization states) to the maximum beat note power available $P^{\Delta\nu}_{proj}$, which is obtained when the two eigen polarization states are maximally projected at the laser output by inserting a polarizer (transmission T_p = 85%) at a 45° angle with respect to the illumination polarization directions. This contrast was derived from the corresponding electrical spectra analyzed around frequency $\Delta\nu$ on the ESA, as illustrated in Fig. 2(b). The results are summarized in Table 1.

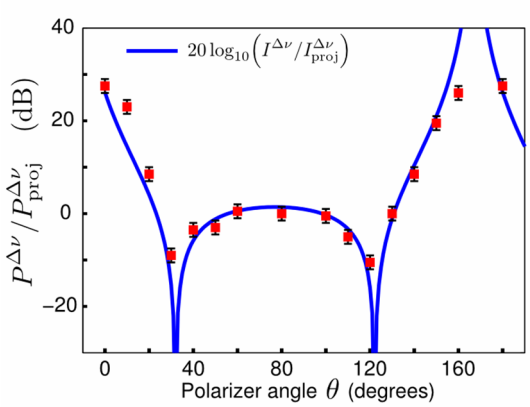

Figure 3. Polarimetric orthogonality contrast measured on a rotating polarizer and mirror.

It can be seen from these results that orthogonality is fairly well maintained during propagation over tens of kilometers, which is strongly encouraging for endoscopic operation. It was also observed that the circulator was rather detrimental to

orthogonality, and that an effort should be made on this component to minimize induced spurious orthogonality breaking on the circulator. More importantly, it is interesting to note that this first validation setup made it possible to measure values of $\mathcal{P}$ up to 99.5% since offering a 25 dB dynamics range (99.95% with 30 dB dynamics). The DSOB technique may therefore prove particularly efficient when slight depolarization contrasts have to be characterized. Further calibration was also conducted on a well-controlled dichroic sample. For that purpose, the setup of Fig. 2 was used with a fibered collimator to illuminate a rotating polarizer in free-space (axis θ_0=32°) followed by a mirror. The polarimetric contrast of the light back propagated into the fiber was analyzed on the spectrum analyzer for various orientations of the polarizer. The obtained results are plotted in Fig. 3 and are in fair agreement with theoretical predictions that can be derived from the equations given in Section 3, provided the intensity reflected at the fiber or collimator ends is taken into account [14].

4.3. Validation on test samples

The setup described above was tested on a variety of test targets in order to validate experimentally the DSOB technique in an endoscopic configuration. The targets under investigation were placed in the vicinity of the FC-APC fiber-end connector without any collimation optics. In such conditions, a very weak proportion of the illumination optical power was backscattered into the fiber mode and propagated to the detector: ≅10 µW on a metallic adhesive sample and only ≅0.7 µW on a diffusive paper sheet. This drawback was however compensated by the high detectivity level of the technique which involves a heterodyne detection scheme allowing very high sensitivity after amplification of the detected signal and analysis on the ESA. It was first observed that, as expected, the relative beat note optical power was low ($C^{\Delta\nu}_{out}$ =$P^{\Delta\nu}_{out}$/P^{0}_{out} = -22.5 dB +/- 1 dB) on a non-depolarizing medium (metal adhesive, $\mathcal{P}$ ≅ 0.99), whereas it considerably increased (-1.5 dB +/- 1 dB) on a diffusive and depolarizing sample (white paper, $\mathcal{P}$≅ 0.11). It must be noted that in this experiment, the contrast $C^{\Delta\nu}_{out}$ was determined by normalizing the RF output power $P^{\Delta\nu}_{out}$ by $P^{\Delta\nu}_{proj}$ which corresponds to the beat note measured after maximum projection of the output states at 45° of the eigenstates. This quantity is indeed proportional to the overall optical power backscattered by the target (up to a factor T_p =2), and was easier to measure in the experimental context considered. Indeed, it avoids including a DC measurement channel, when simultaneity of the RF and DC measurements is not required, which was the case for this preliminary experiment.

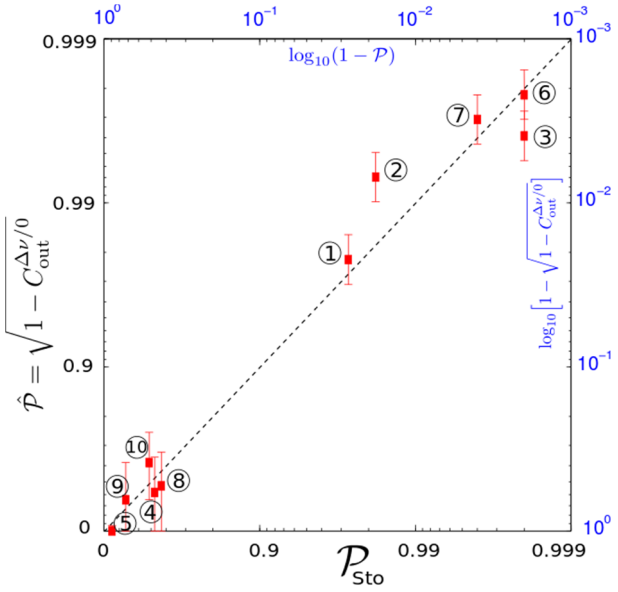

Figure 4. The DOP estimated with the DSOB technique from the measurement of the RF beat note visibility is in fair agreement with standard reference measurements (free-space Stokes measures at 1.55 µm).

We then considered ten samples with distinct depolarization properties, and we compared the DOP estimated with the DSOB technique using Eq. (5), with standard Stokes measurements in free-space at 1.5 µm. This comparison is plotted in Fig. 4 and demonstrates a fair agreement between the DSOB measurements and the reference approach. As a consequence, these experimental results validate the concept of remote depolarization sensing by polarization orthogonality breaking, as well as the DSOB setup proposed. In the next section, we propose another setup architecture in order to perform the first images using DSOB contrasts in the visible range. Moreover, we show that using a lock-in detection to measure precisely the output electrical power at frequency $\Delta\nu$ is advantageous for rapidity and

automation of the measurements. Indeed, the ESA used for the proof of concept in the above setup is not required and could be advantageously replaced by a demodulation circuit since the frequency of interest $\Delta\nu$ is known.

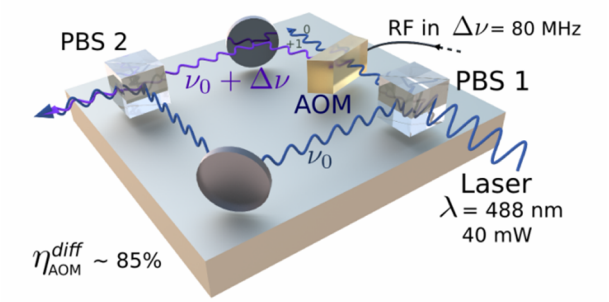

Figure 5. Dual-frequency source at 488nm for imaging experiments.

5. First DSOB images in free-space in the visible

More recently, we implemented the DSOB technique on a free-space setup in order to obtain the first polarimetric images with this novel technique. For that purpose, we used a confocal microscope setup available in the laboratory, which has been adapted for the sake of the experiment. The operating wavelength selected was λ=488 nm for compatibility with the microscope setup and with biological samples. As a consequence, this led us to design a new source architecture, able to produce the dual-frequency dual orthogonal polarization probe beam at 488 nm. Instead of tackling the difficult (and so far unreported) challenge consisting in designing a dual frequency laser at 488 nm with sufficient power, we proposed to use a 40 mW commercial 488 nm monomode source. This source was then injected in free-space into a two-arms polarization splitting/ combining setup, represented in Fig. 5, and comprising an acousto-optics modulator (AOM) in one of the arms so as to ensure a fixed frequency difference $\Delta\nu$=80 MHz (diffraction efficiency of about 85 %). Such setup allows preparation of a dual frequency orthogonal polarization beam, but at the expense of strong requirements in mechanical stability and beam alignment. Moreover, the polarimetric contrast and modes overlapping at the source output is necessarily imperfect (about 80% maximum polarization contrast) in comparison to a true dual-frequency source in which the two modes share the same resonant cavity. However, using a commercial monomode source ensures high power and good stability in time, which is necessary for spatially resolved measurements on a target.

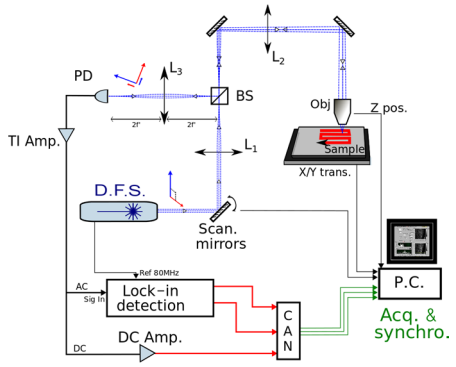

Figure 6. Schematic of the confocal microscope setup and detection modules. (DFS: dual-frequency source).

As represented in Fig. 6, this probe beam was then injected in the microscope setup using a telescopic lens arrangement, and a final x4 objective with limited numerical aperture (NA=0.1) was used to shine the sample with an optical power of about 5 mW. The detection of light scattered by the sample in a reflective geometry was performed through a polarization-insensitive beamsplitter which played the role of the circulator used in the fibred setup. Light was detected on a fast Hamamatsu Si photodiode (bandpass typ. 100 MHz), which acted as a confocal pinhole. The output intensity was amplified with a transimpedance electrical amplifier which fed a 200 MHz lock-in detection (Stanford Research). The demodulation was performed using the reference RF frequency at 80 MHz driving the AOM, and a digital-to-analogic converter (DAC) was used to display the measurement results to a computer which controlled the experiment. Typical integration times of 30 ms were used in these first experiments, which allowed a 2,25 k.pixels image to be recorded in about 67 s, using an X/Y precision translation stage (10 mm/s). In the forthcoming experiments, galvanometric mirrors will be implemented to ensure faster raster scanning of the samples. In addition to the AC intensity component at 80 MHz, it was also necessary to record the DC component,

which was operated through a low-frequency voltage amplifier feeding another port of the DAC.

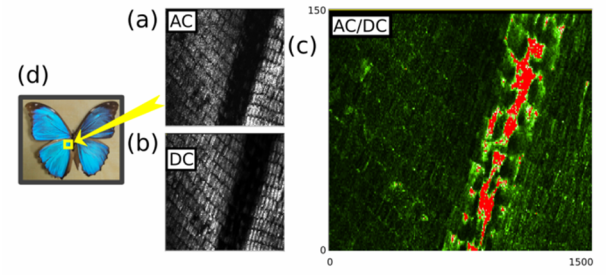

Figure 7. First DSOB images obtained on a morpho butterfly wing (d). The contrast ratio image (c) is obtained from the AC image retaining beat note intensity at 80 MHz (a) and from the DC (standard intensity) image (b).

This setup made it possible to obtain the first polarization contrast images using the DSOB technique in a free-space configuration at 488 nm. An example of such acquisitions is given in Fig. 7, in which we display the DC image in Fig. 7.(a) (corresponding to standard intensity measurements), along with the AC component at 80 MHz (Fig. 7.(b)), used to compute the contrast ratio image given in Fig. 7.(c). It can be observed that on the sample considered (portion of wing of Morpho butterfly, see Fig. 7. (d)), the DSOB contrast image reveals contrasts which are not visible in the standard intensity image. More precisely, it can be seen that the central region seems to exhibit strongly depolarizing/dichroic behavior. These preliminary imaging results have to be refined and studied more thoroughly in the future. For instance, a better calibration procedure must be defined so as to avoid unwanted saturations in the contrast ratio images, as in Fig. 7.(c). These results are however very encouraging for future implementation of the DSOB technique as a single-shot characterization of polarimetric response of a sample with very short acquisitions times.

6. Conclusions and perspectives

The novel technique that has been addressed in this article provides a direct characterization of the depolarization properties of a sample with unprecedented sensitivity and rapidity in comparison to existing polarimetric sensing devices (< 1 µs/pixel is feasible with high freqency detuning and optimized demodulation electronics). Such capacity is thus expected to enable the development of real-time long-range polarimetric imaging systems with unprecedented sensitivity and rapidity. Moreover, by providing a technical solution to remote-sensing through optical fibers, this technique will open a new set of applications for defense. Such capability could indeed be of interest for discreet surveillance imaging systems, by physically separating emission/detection modules from beam forming optics. Using galvanometric mirror scanning and image reconstruction could easily lead to high-repetition rate polarimetric imaging (>10 Hz). Lastly, sensing applications for distant optical interrogation of sensors in hostile environments could be triggered by use of specific materials exhibiting induced diattenuation/depolarization effects. Among other assets for military surveillance applications, the spectral agility offered by the technique has to be validated on realistic scenarios. In case of success, this may thus enable the development of new generations of spectro-polarimetric imagers over much wider spectral extent.

Acknowledgments

This work has been partly funded by the CNRS *Mission for Interdisciplinarity* through the IMPOLABO project. Upcomings studies are partially funded by the French National Defense Agency (DGA/ANR).

7. REFERENCES

1. Alouini, M *et al.* (2004). Multispectral polarimetric imaging with coherent illumination: towards higher image contrast. In Defense and Security, International Society for Optics and Photonics, pp. 133-144

2. Alouini M., Roux N., Le Hors L., Hartemann P., Breugnot S., Dolfi D. (2008). Active spectro-polarimetric imaging: signature modeling, imaging demonstrator and target detection. *European Physical Journal: Applied Physics* **42**, 129-139.

3. Alouini M., et al. (2009). Near-infrared active polarimetric and multispectral laboratory demonstrator for target detection. *Applied Optics* **48**, 1610.

4. Bartlett, B. D., Gartley, M. G., Messinger, D. W., Salvaggio, C., & Schott, J. R. (2010). Spectro-polarimetric bidirectional reflectance distribution function determination of in-scene materials and its use in target detection applications. *Journal of Applied Remote Sensing* **4** (1), 43552-43552.

5. Bénière A., Alouini M., et al. (2010). Snapshot active polarimetric and multispectral laboratory demonstrator for land mine detection. in International symposium on optronics in defense and security, OPTRO.

6. Goudail F., Roux N., Baarstad I., Loke T., Kaspersen P., Alouini M., Normandin X. (2006). Some practical issues in anomaly detection and exploitation of regions of interest in hyperspectral images. *Applied Optics* **45**, 5223-5236.

7. Meng, L., and Kerekes, J. P. (2011). Adaptive target detection with a polarization-sensitive optical system. *Applied Optics* **50** (13), 1925-1932.

8. H. E. Scott, S. H. Jones, F. J. Iannarilli, and K. Annen, (1998). Hyperspectral IR polarimetry with applications in demining and unexploded ordnance detection. in Proc. SPIE 3534, 300-320.

9. Tyo, J. S., Goldstein, D. L., Chenault, D. B., and Shaw, J. A. (2006). Review of passive imaging polarimetry for remote sensing applications. *Applied Optics* **45** (22), 5453-5469.

10. Denes, L. J., Gottlieb, M., Kaminsky, B. and Huber, D. F. (1998). Spectro-polarimetric imaging for object recognition. in Proc. SPIE 3240, 8-18.

11. P. Eliès, B. Le Jeune, M. Floc'h, and J. Lotrian. (1997). Depolarization classification of metallic and dielectric targets. In Proc. SPIE 3059, 174.

12 Gupta, N., Denes, L. J., Gottlieb, M., Suhre, D. R., Kaminsky, B., Metes, P. (2001). Object detection with a field-portable spectropolarimetric imager. *Applied Optics* **40** (36), 6626-6632.

13. L. Le Hors, P. Hartemann, and S. Breugnot. (2000). Multispectral polarization active imager in the visible band. In Proc. SPIE 4035, 380-389.

14. J. Fade and M. Alouini. (2012). Depolarization remote sensing by orthogonality breaking. *Physical Review Letters* **109**, 043901.

15 Aït-Belkacem, D., Gasecka, A., Munhoz, F., Brustlein, S. and Brasselet, S. (2010). Influence of birefringence on polarization resolved nonlinear microscopy and collagen SHG structural imaging. *Optics Express* **18** (14), 14859-14870.

16. Brasselet, S. (2011). Polarization-resolved nonlinear microscopy: application to structural molecular and biological imaging. *Advances in Optics and Photonics* **3** (3), 205-271.

17. Latour, G., Gusachenko, I., Kowalczuk, L., Lamarre, I., & Schanne-Klein, M. C. (2012). In vivo structural imaging of the cornea by polarization-resolved second harmonic microscopy. *Biomedical Optics Express* **3** (1), 1-15.

18. P. Terrier, V. Devlaminck and J.M. Charbois. (2008). Segmentation of rough surfaces using a polarization imaging system. *J. Opt. Soc. Am. A* **25**, 423-430.

19 Lefebvre, J., & Finnie, P. (2011). Polarized light microscopy and spectroscopy of individual single-walled carbon nanotubes. *Nano Research* **4** (8), 788-794.

20. D.T. Cassidy, S.K.K. Lam, B. Lakshmi and D.M. Bruce. (2004). Strain Mapping by Measurement of the Degree of Polarization of Photoluminescence. *Appl. Opt*. **43**, 1811-1818.

21. Wolff, L. B. (1994). Polarization camera for computer vision with a beam splitter. *JOSA A* **11** (11), 2935-2945.

22. Emile O., Bretenaker F. and Le Floch A. (1996). Rotating polarization imaging in turbid media. *Opt. Lett.* **21**, 1706-1708.

23. Ramachandran H. and Narayanan A. (1998). Two-dimensional imaging through turbid media using a continuous wave light source. *Opt. Commun*. **154**, 255-260.

24. M S. Breugnot and P. Clémenceau. (1999). Modeling and performances of a polarization

active imager at λ=806 nm. In Proc. SPIE 3707, 449-460.

25. Sadjadi, F. A., & Chun, C. L. (2003). Automatic detection of small objects from their infrared state-of-polarization vectors. *Optics letters* **28** (7), 531-533.

26. M. Anastasiadou, *et al.* (2008). Polarimetric imaging for the diagnosis of cervical cancer. *Phys. Status Solidi C* **5**, 991-999.

27. F. Boulvert, B. Boulbry, G. Le Brun, B. Le Jeune, S. Rivet, and J. Cariou. (2005). Analysis of the depolarizing properties of irradiated pig skin. *Journal of Optics A: Pure and Applied Optics* **7**, 21.

28. A. De Martino, Y.-K. Kim, E. Garcia-Caurel, B. Laude, and B. Drévillon. (2003). Optimized Mueller polarimeter with liquid crystals. *Opt. Lett*. **28**, 616-618.

29. Groner, W., Winkelman, J. W., Harris, A. G., Ince, C., Bouma, G. J., Messmer, K., & Nadeau, R. G. (1999). Orthogonal polarization spectral imaging: a new method for study of the microcirculation. *Nature medicine* **5**, 1209-1213.

30. Ortega-Quijano, N., Fanjul-Vélez, F., de Cos-Pérez, J., & Arce-Diego, J. L. (2011). Analysis of the depolarizing properties of normal and adenomatous polyps in colon mucosa for the early diagnosis of precancerous lesions. *Optics Communications* **284** (19),4852-4856.

31. I. Semenovitch, F. Sicuro, O. Lupi, and E. Bouskela. (2011). Evaluation of basal cell carcinoma microcirculation through orthogonal polarization technique. *Archives of Dermatological Research* **303**, 475-479.

32. M. H. Smith, P. Burke, A. Lompado, E. Tanner, L. W. Hillman. (2000). Mueller matrix imaging polarimetry in dermatology. In Proc. SPIE 3911, 210.

33. M. Z. Tannous, M. Al-Arashi, S. Shah, and A. N. Yaroslavsky. (2009). Delineating melanoma using multimodal polarized light imaging. Lasers in Surgery and Medicine **41**, 10-16.

34. Réfrégier P., Fade J., Roche M. (2007). Estimation precision of the degree of polarization from a single intensity image. *Optics Letters* **32**, 739-741.

35. Roche M., Fade J., Réfrégier P. (2007). Parametric estimation of the square degree of polarization from two intensity images degraded by fully developed speckle noise. *Journal of the Optical Society of America A* **24**, 2719-2727.

36. Collet, E. (1993). Polarized light: fundamentals and applications. *Dekker, New-York*.

37. Goudail, F., and Réfrégier, P. (2004). Statistical image processing techniques for noisy images: an application-oriented approach. *Springer*.

38. Fade, J., Roche, M. and Alouini, M. (2012). Computational polarization imaging from a single speckle image. *Optics Letters* **37** (3), 386-388.

39. Brunel, M., Emile, O., Bretenaker, F., LeFloch, A., Ferrand, B., & Molva, E. (1997). Tunable two-frequency lasers for lifetime measurements. *Optical Review* **4** (5), 550-552.

40. Baili, G., Morvan, L., Alouini, M., Dolfi, D., Bretenaker, F., Sagnes, I., & Garnache, A. (2009). Experimental demonstration of a tunable dual-frequency semiconductor laser free of relaxation oscillations. *Optics letters* **34** (21), 3421-3423.